Available online at www.sciencedirect.com
ScienceDirect
Physics Letters B 642 (2006) 203–209
PHYSICS LETTERS B
www.elsevier.com/locate/physletb

Study of $\phi \to \pi^+\pi^-\pi^0$ with CMD-2 detector

R.R. Akhmetshin [a], V.M. Aulchenko [a,b], V.Sh. Banzarov [a], L.M. Barkov [a,b], N.S. Bashtovoy [a], A.E. Bondar [a], D.V. Bondarev [a,b], A.V. Bragin [a], S.I. Eidelman [a,b], D.A. Epifanov [a,*], G.V. Fedotovich [a,b], N.I. Gabyshev [a], D.A. Gorbachev [a], A.A. Grebeniuk [a], D.N. Grigoriev [a,b], F.V. Ignatov [a], S.V. Karpov [a], V.F. Kazanin [a,b], B.I. Khazin [a,b], I.A. Koop [a,b], P.P. Krokovny [a,b], A.S. Kuzmin [a,b], I.B. Logashenko [a,c], P.A. Lukin [a], A.P. Lysenko [a], K.Yu. Mikhailov [a], A.I. Milstein [a,b], I.N. Nesterenko [a,b], M.A. Nikulin [a], V.S. Okhapkin [a], A.V. Otboev [a], E.A. Perevedentsev [a,b], A.S. Popov [a], S.I. Redin [a], N.I. Root [a], A.A. Ruban [a], N.M. Ryskulov [a], Yu.M. Shatunov [a], B.A. Shwartz [a,b], A.L. Sibidanov [a], V.A. Sidorov [a], A.N. Skrinsky [a], V.P. Smakhtin [d], I.G. Snopkov [a], E.P. Solodov [a,b], Yu.V. Yudin [a], A.S. Zaitsev [a,b], S.G. Zverev [a]

[a] *Budker Institute of Nuclear Physics, Russian Acad. Sci. Siberian Div., Novosibirsk 630090, Russia*
[b] *Novosibirsk State University, Novosibirsk 630090, Russia*
[c] *Boston University, Boston, MA 02215, USA*
[d] *Weizmann Institute of Science, 76100 Rehovot, Israel*

Received 21 July 2006; accepted 13 September 2006

Available online 4 October 2006

Editor: M. Doser

Abstract

The cross section of the process $e^+e^- \to \pi^+\pi^-\pi^0$ has been measured in the c.m. energy range 984–1060 MeV with the CMD-2 detector at the VEPP-2M collider. The obtained value of $Br(\phi \to e^+e^-)Br(\phi \to \pi^+\pi^-\pi^0) = (4.51 \pm 0.16 \pm 0.11) \times 10^{-5}$ is in good agreement with the previous measurements and has the best accuracy. Analysis of the Dalitz plot was performed. The contributions of the dominant $\phi \to \rho\pi$ mechanism as well as of a small direct $\phi \to 3\pi$ amplitude were determined.

PACS: 12.40.Vv; 13.25.Gv; 13.66.Bc; 13.66.Jn; 14.40.Ev

1. Introduction

A study of e^+e^- annihilation into hadrons at low energies has a long history, but despite decades of experiments, new precise measurements are still interesting and can provide important information about interactions of light quarks and spectroscopy of their bound states.

This work is devoted to a study of the process $e^+e^- \to \pi^+\pi^-\pi^0$ within the ϕ-meson energy range with the CMD-2 detector [1,2] at the VEPP-2M e^+e^- collider [3] in the Budker Institute of Nuclear Physics (Novosibirsk).

It was suggested long time ago by Gell-Mann, Sharp and Wagner [4] that $\phi \to \pi^+\pi^-\pi^0$ decay proceeds via the $\rho\pi$ intermediate state. First evidence of $\rho\pi$ dominance was obtained in [5]. Later, experiments with the CMD-2 [6] and SND [7] detectors confirmed this conclusion and set upper limits on the non-$\rho\pi$ amplitude. However, some phenomenological models, for example, the effective Lagrangian approach [8–10], HLS [11] predict a contact term in this decay. Recently new results on $\phi \to \pi^+\pi^-\pi^0$ from the KLOE experiment [12] as well as preliminary results from the CMD-2 detector [13] were reported. The final results of the latter experiment are presented here.

* Corresponding author.
E-mail address: d.a.epifanov@inp.nsk.su (D.A. Epifanov).

0370-2693/$ – see front matter
doi:10.1016/j.physletb.2006.09.041

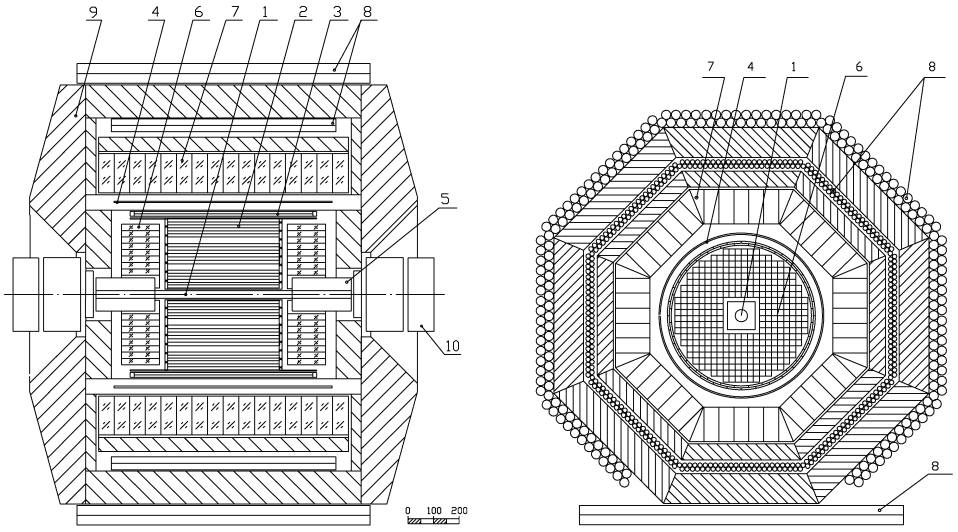

Fig. 1. Layout of CMD-2. 1—beam pipe; 2—drift chamber (DC); 3—Z-chamber (ZC); 4—superconducting solenoid; 5—compensating solenoid; 6—BGO endcap calorimeter; 7—CsI barrel calorimeter; 8—muon range system; 9—iron yoke; 10—quadrupole lenses.

One more important issue of this work is a precise measurement of the cross section $\sigma_{3\pi}(E)$, the $\phi \to \pi^+\pi^-\pi^0$ branching ratio as well as parameters of ϕ–ω mixing. This information is important for the precise evaluation of the hadronic contribution to the muon anomalous magnetic moment $(g-2)_\mu$ [14] and for a test of various mixing models [15].

2. CMD-2 detector

The layout of CMD-2 (Cryogenic Magnetic Detector) is shown in Fig. 1. This general-purpose detector combines features of a spectrometer for detection of charged particles with good calorimetry for photons.

The tracking part of the detector consists of a cylindrical drift chamber (DC) and double-layer multiwire proportional chamber (Z-chamber). Outside the superconducting solenoid with a 1 T magnetic field a barrel electromagnetic calorimeter based on CsI scintillation crystals and muon range system are placed. To keep good energy resolution of the barrel calorimeter, the solenoid design was optimized to have a small thickness, 0.38 X_0. The endcap calorimeter is made of BGO scintillation crystals. Together, the barrel and endcap calorimeters cover a solid angle of $0.92 \times 4\pi$ steradians.

This analysis of the process $e^+e^- \to \pi^+\pi^-\pi^0$ is based on the experimental information collected at the CMD-2 detector with integrated luminosity of about 11 pb^{-1}. The data were taken at 54 points in the center-of-mass energy range from 984 to 1060 MeV by three scans.

3. Selection of $\pi^+\pi^-\pi^0$ events

The cross section measurement as well as Dalitz plot studies were based on fully reconstructed 3π events. Partially reconstructed events were used to determine corrections to the detection efficiency. The main data sample contains events with two charged particles (one positive and one negative) and two or more reconstructed photon clusters selected by the following criteria: All charged particles are required to hit the detector within the solid angle limited by the polar angle $|\pi/2 - \theta| < 0.67$ radians to provide high efficiency track reconstruction both in Z-chamber and DC. The same criterion was applied to the polar angles of γ-quanta to avoid edge effects for the detection efficiency in the CsI calorimeter. For charged particles:

- For each track the spread of the hits from the optimal helix in the $(R$–$\varphi)$ plane $\sigma_R < 0.1$ cm and in the $(R$–$Z)$ plane $\sigma_Z < 3$ cm (to be compared with the average spatial resolution of the DC: $\sigma_R < 0.025$ cm and $\sigma_Z < 0.4$ cm in the transverse and longitudinal directions).
- Tracks should be acollinear in the $(R$–$\varphi)$ projection $|\pi - |\varphi_2 - \varphi_1|| > 0.1$ to reject Bhabha events and a space angle between tracks should be $0.1 < \psi < 3.0$ to reject events of γ conversion in the wall of the beam pipe.
- The closest approach of each track to the beam axis should be $R_{\min} < 0.2$ cm in the $(R$–$\varphi)$ projection while the distance from a track to the interaction point along the beam direction should be $|Z_{\rm trk}| < 10$ cm.
- The momentum of each track is required to be $P_\pi < 500$ MeV$/c$.
- To reject events with initial state radiation (ISR) of a hard photon we apply a cut on the absolute value of the 3π system total momentum $|\vec{P}_{\pi^+} + \vec{P}_{\pi^-} + \vec{P}_{\pi^0}| < 100$ MeV$/c$.
- Specific ionization losses in the DC should be $dE/dx < 2(dE/dx)_{\rm MIP}$ to suppress charged kaons.

A neutral pion was identified by two photons with the energy of $E_\gamma > 30$ MeV each and invariant mass in the range of $80 < M_{\gamma\gamma} < 170$ MeV$/c^2$. If more than two photons were detected, we selected events where only one π^0 candidate was found among all $\gamma\gamma$ combinations, $N_{\pi^0} = 1$. Fig. 2 shows the P_{π^+} versus P_{π^-} scatter plot of the selected experimental events at $E_{\rm beam} = 509.5$ MeV.

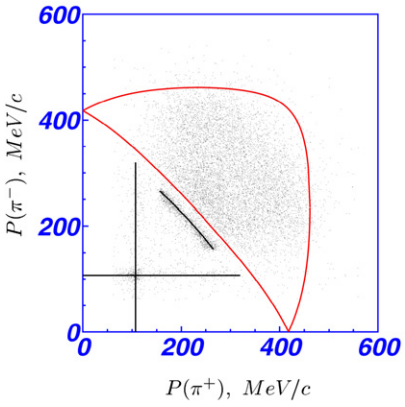

Fig. 2. The P_+ vs. P_- scatter plot of the data at $E_{\text{beam}} = 509.5$ MeV. Also shown are: the $\pi^+\pi^-\pi^0$ allowed kinematic region, the calculated curve of $P_+(P_-)$ dependence for $K_L K_S$ events and two lines indicating location of K^+K^- events.

Clearly seen are events of three types: $\pi^+\pi^-\pi^0$ inside the allowed kinematic region; $K_L K_S$, where $K_S \to \pi^+\pi^-$ events are along the calculated curve of $P_+(P_-)$ dependence; K^+K^- events along two lines with $P(K^\pm) = 107$ MeV. Charged particles from the $K^\pm \to \mu^\pm\nu_\mu$ decay can have momenta in the large range up to the 310 MeV/c. Two lines show the location of the events with one kaon decaying to lighter particles. Finally, we selected events above the lower boundary of the 3π allowed kinematic region to suppress events of $\phi \to K_S K_L$ decay, and applied a cut on the track momentum $P_\pi > 120$ MeV/c to reject events of $\phi \to K^+K^-$ decay. With the above criteria, 104 849 events were selected in the c.m. energy range $\sqrt{s} = 984$–1060 MeV.

4. Background

The background for the studied decay mode can originate from true e^+e^- interactions or from cosmic particles and beam interactions with the residual gas. This contribution was evaluated considering events from the sideband region $10 < |Z_{\text{trk}+}| < 20$ cm, and found to be negligible (less than 0.1%). MC simulation showed that the total background contamination is about 1% at the ϕ-meson peak and increases up to 20% at the edge of the studied energy range. To evaluate the number of background events coming from e^+e^- processes, we studied the $\gamma\gamma$ invariant mass distribution of π^0 candidates. Signal events group around the π^0 mass, while the $\gamma\gamma$ distribution of background events is flat for all background processes excluding $e^+e^- \to \pi^+\pi^-\pi^0\pi^0$ and $e^+e^- \to \phi \to \eta\gamma$, $\eta \to \pi^+\pi^-\pi^0$ processes (the contribution of the latter was found to be negligible). To extract the number of signal events at each energy point the $\gamma\gamma$ invariant mass distribution was approximated by a sum of a logarithmic Gaussian and a constant term. The mean value, width, asymmetry of logarithmic Gaussian as well as the fraction of signal events with wrong reconstructed π^0 having a flat $\gamma\gamma$ distribution, were fixed at their values found from the approximation at the ϕ-meson peak, where background is small ($\sim 1\%$) and can be found from MC. The fraction of $e^+e^- \to \pi^+\pi^-\pi^0\pi^0$ events having a peak in the $\gamma\gamma$ distribution was calculated from the luminosity, cross section [16] and MC efficiency. The detailed description of the procedure can be found in [17].

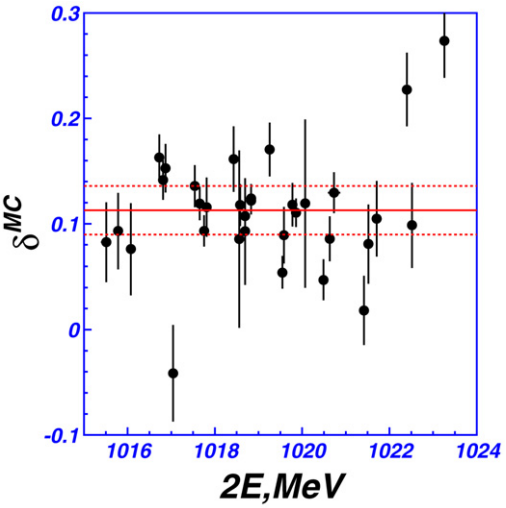

Fig. 3. Efficiency correction δ^{MC} for c.m. energies close to the ϕ-meson mass. For the other points the average value $\delta^{\text{MC}} = 0.113 \pm 0.023$ is used.

5. Detection efficiency

The value of the $\pi^+\pi^-\pi^0$ detection efficiency, $\varepsilon_{3\pi}^{\text{MC}} = (4.71 \pm 0.02)\%$, was obtained using a large MC sample of 10^6 generated $e^+e^- \to \pi^+\pi^-\pi^0$ events at the c.m. energy $\sqrt{s} = 1019.5$ MeV. However, Monte Carlo simulation cannot reproduce all details of the detector response. The corrections $\delta_{\text{trk}}^{\text{MC}}(s)$ were introduced to take into account the difference between the track efficiency in Monte Carlo and the experimental one. These values were determined by comparing the numbers of selected events in the sample with one track and one π^0 and with two tracks and π^0. Similar procedure was used to determine π^0 efficiency corrections $\delta_{\pi^0}^{\text{MC}}(s)$. The details of these procedures can be found in [17]. The total correction δ^{MC} at each energy point, determined by the formula:

$$\left(1-\delta^{\text{MC}}\right) = \left(1-\delta_{\text{trk}-}^{\text{MC}}\right)\left(1-\delta_{\text{trk}+}^{\text{MC}}\right)\left(1-\delta_{\pi^0}^{\text{MC}}\right), \tag{1}$$

is shown in Fig. 3.

6. Cross section

A visible cross section of the process $e^+e^- \to \pi^+\pi^-\pi^0$ is calculated according to the formula:

$$\sigma_{\text{vis}} = \frac{N_{3\pi}}{\mathcal{L}\varepsilon_{\text{trig}}\varepsilon_{3\pi}^{\text{MC}}(1+\delta_{\text{wid}})(1-\delta^{\text{MC}})} = (1+\delta_{\text{rad}})\sigma_{\text{B}}, \tag{2}$$

where: $N_{3\pi}$—number of 3π events, $\mathcal{L}$—integrated luminosity, $\varepsilon_{\text{trig}}$—trigger efficiency, $\varepsilon_{3\pi}^{\text{MC}}$—$3\pi$ MC detection efficiency, δ^{MC}—efficiency correction, δ_{wid} takes into account the effect of the beam energy spread ($\sigma_E = 300$ keV), σ_{B}—3π Born cross section, δ_{rad}—correction due to the initial state radiation. Table 1 shows the values of σ_{vis} and σ_{B} for different c.m. energies. The value of $\varepsilon_{\text{trig}}$ is determined from the experimental data sets,

Table 1
The experimental results for 3 energy scans. $E_{\rm beam}$—beam energy, $\mathcal{L}$—luminosity, $N_{\rm sel}$—number of selected events, $\sigma_{\rm vis}$—visible cross section, $\sigma_{\rm B}$—Born cross section

#	$E_{\rm beam}$, MeV	$\mathcal{L}$, nb^{-1}	$N_{\rm sel}$	$\sigma_{\rm vis}$, nb	$\sigma_{\rm B}$, nb
Scan 1					
1	509.347 ± 0.016	29.91	560	449.35 ± 34.91	613.72 ± 47.78
2	509.279 ± 0.028	9.25	162	447.47 ± 60.03	613.67 ± 82.61
3	492.010 ± 0.300	110.54	87	16.52 ± 2.55	19.01 ± 2.94
4	502.000 ± 0.300	115.50	148	21.73 ± 3.29	26.58 ± 4.26
5	505.299 ± 0.060	165.12	374	47.77 ± 3.73	61.17 ± 4.92
6	508.038 ± 0.012	111.62	849	171.75 ± 11.05	234.66 ± 15.27
7	508.434 ± 0.011	237.80	2439	264.92 ± 9.70	365.45 ± 13.70
8	508.906 ± 0.011	111.13	1625	356.99 ± 16.04	494.74 ± 22.56
9	509.628 ± 0.017	126.76	2185	459.51 ± 18.88	611.44 ± 25.23
10	508.769 ± 0.007	253.78	3325	334.98 ± 10.57	464.25 ± 14.86
11	509.216 ± 0.008	75.27	1262	452.68 ± 22.81	622.74 ± 31.47
12	509.289 ± 0.004	234.92	4162	447.12 ± 13.42	612.83 ± 18.43
13	509.345 ± 0.010	67.83	1205	433.91 ± 23.73	592.69 ± 32.47
14	509.792 ± 0.006	117.34	2186	460.68 ± 18.25	599.69 ± 23.83
15	509.888 ± 0.008	227.89	3945	434.95 ± 13.39	557.75 ± 17.36
16	510.316 ± 0.007	224.74	3171	322.96 ± 10.44	382.04 ± 12.58
17	510.760 ± 0.010	117.25	1107	216.75 ± 11.81	232.47 ± 12.83
18	511.199 ± 0.008	163.78	986	163.97 ± 9.72	158.84 ± 9.50
19	513.730 ± 0.032	180.87	318	37.30 ± 3.06	18.98 ± 1.65
20	516.721 ± 0.100	152.85	118	17.15 ± 2.07	3.66 ± 0.62
21	519.782 ± 0.043	126.89	68	11.20 ± 1.87	0.81 ± 0.20
22	529.803 ± 0.072	179.81	79	3.52 ± 1.55	0.20 ± 0.20
Scan 2					
23	505.217 ± 0.060	157.41	350	52.12 ± 3.75	66.65 ± 4.93
24	507.892 ± 0.012	142.25	1027	169.64 ± 9.38	230.87 ± 12.91
25	508.362 ± 0.007	269.42	2610	246.59 ± 8.80	339.65 ± 12.26
26	508.827 ± 0.004	433.23	5862	336.58 ± 8.23	466.54 ± 11.50
27	509.414 ± 0.005	579.24	10272	460.78 ± 9.04	626.24 ± 12.33
28	509.929 ± 0.002	582.46	9810	414.82 ± 8.30	528.37 ± 10.64
29	510.366 ± 0.070	351.00	4397	304.01 ± 8.91	355.90 ± 24.00
30	510.855 ± 0.050	156.80	1235	181.77 ± 9.69	190.74 ± 13.57
31	511.629 ± 0.011	227.48	971	119.89 ± 7.58	104.72 ± 6.69
32	514.061 ± 0.018	178.05	273	32.23 ± 2.90	15.00 ± 1.42
33	516.960 ± 0.028	163.09	123	16.53 ± 2.02	3.26 ± 0.57
34	519.875 ± 0.063	178.59	120	12.64 ± 1.84	0.88 ± 0.21
35	525.046 ± 0.059	210.27	100	5.62 ± 1.43	0.10 ± 0.10
Scan 3					
36	502.000 ± 0.300	168.29	239	29.35 ± 2.88	35.90 ± 3.79
37	492.000 ± 0.300	194.78	153	14.27 ± 1.93	16.43 ± 2.22
38	502.000 ± 0.300	158.57	216	28.32 ± 2.94	34.64 ± 3.86
39	505.020 ± 0.300	163.42	350	47.02 ± 3.73	59.92 ± 7.20
40	507.756 ± 0.060	144.69	957	151.72 ± 8.77	205.71 ± 14.65
41	508.406 ± 0.050	402.70	4176	259.70 ± 7.60	358.05 ± 17.39
42	508.878 ± 0.004	462.62	6906	358.41 ± 8.08	496.77 ± 11.31
43	509.415 ± 0.005	415.08	7478	468.55 ± 10.03	636.74 ± 13.67
44	509.774 ± 0.006	401.18	7691	458.07 ± 9.93	597.86 ± 13.08
45	510.244 ± 0.005	318.17	4758	329.95 ± 9.03	396.19 ± 10.98
46	510.707 ± 0.007	174.65	1662	195.80 ± 8.98	212.55 ± 9.89
47	511.258 ± 0.017	156.43	893	124.46 ± 7.81	118.91 ± 7.70
48	513.735 ± 0.020	210.87	342	36.71 ± 2.72	18.65 ± 1.47
49	516.691 ± 0.026	203.74	195	17.76 ± 2.12	3.82 ± 0.64
50	519.708 ± 0.043	147.07	82	7.10 ± 1.88	0.52 ± 0.17
51	524.617 ± 0.061	106.68	56	8.34 ± 2.01	0.14 ± 0.14
52	529.503 ± 0.080	59.73	20	8.97 ± 2.37	0.48 ± 0.47
53	508.521 ± 0.040	73.70	921	255.06 ± 15.33	352.44 ± 24.37
54	510.035 ± 0.040	15.07	243	409.74 ± 48.82	512.23 ± 62.52

triggered by a signal from one of the two independent subsystems (CsI or DC), and by a signal from both subsystems. It was found to be higher than 98% for all c.m. energies. The procedure is discussed in detail in [17].

Table 2
Results of the visible cross section approximation

Parameters	Fit 1	Fit 2
m_ϕ, MeV/c^2	$1019.30 \pm 0.02_{\rm stat} \pm 0.10_{\rm syst}$	1019.33 ± 0.03
Γ_ϕ, MeV	$4.30 \pm 0.06_{\rm stat} \pm 0.17_{\rm syst}$	4.26 ± 0.06
$\varphi_{\phi-\omega}$	$167^\circ \pm 14^\circ_{\rm stat} \pm 10^\circ_{\rm syst}$	180°-fixed
$\sigma_{3\pi}$, nb	$637 \pm 23_{\rm stat} \pm 16_{\rm syst}$	658 ± 7
$A_{\rm add}$, $\sqrt{\rm nb}$/MeV^2	0-fixed	22 ± 8
χ^2/Ndf	57.0/50	51.8/50
$P(\chi^2)$, %	23	40

The important issue for the evaluation of $\sigma_{\rm B}$ is an accurate account of the radiative corrections. In this work the approach developed in [18] was used which assumes that both electron and positron emit photon jets in the forward direction. In this case the visible cross section is related to $\sigma_{\rm B}$ as

$$\sigma_{\rm vis}(s) = \int_0^1 dx_1 \int_0^1 dx_2\, D(x_1,s)D(x_2,s)\sigma_{\rm B}(s')\varepsilon(x_1,x_2) = \big(1+\delta_{\rm rad}(s)\big)\sigma_{\rm B}(s), \quad (3)$$

where: $D(x_{1,2},s)$—the probability function for initial $e^\pm$ to emit a γ-quantum jet carrying $x_{1,2}$ part of $e^\pm$ energy $\sqrt{s}/2$, $\sigma_{\rm B}(s')$—3π Born cross section at $s' = s(1-x_1)(1-x_2)$, $\varepsilon(x_1,x_2)$—efficiency function, which is defined as a detection efficiency for a boosted (due to γ-quantum radiation) $\pi^+\pi^-\pi^0$ system normalized to that at $x_1 = x_2 = 0$ and calculated using 3π MC simulation of 10^6 events with initial state radiation. The Born cross section is dominated by the ω and ϕ contributions:

$$\sigma_{\rm B}(s) = \frac{F_{3\pi}(s)}{s}\big|A_\omega + A_\phi e^{i\delta_{\phi-\omega}} + A_{\rm add}\big|^2, \quad (4)$$

where: A_ω, A_ϕ—ω and ϕ meson amplitudes, $\delta_{\phi-\omega}$—ϕ–ω interference phase, and the constant term $A_{\rm add}$ takes into account the contributions of the higher mass vector resonances (such as ω' and ω'') around the ϕ-meson. The detailed description of the A_ω, A_ϕ parametrization can be found elsewhere [6,15,17].

The experimental $\sigma_{\rm vis}(s)$ values were approximated by the function given by Eq. (3). Table 2 shows the results of two fits.

For both fits the ϕ-meson mass m_ϕ, its width Γ_ϕ and 3π peak cross section $\sigma_{3\pi}$ were free parameters. However, our sensitivity is not sufficient to keep free both $\varphi_{\phi-\omega}$ and $A_{\rm add}$. So $\varphi_{\phi-\omega}$ is free in the Fit 1 and fixed at 180° in the Fit 2. All the other parameters were fixed at their world average values [19] within their uncertainties. Fig. 4 demonstrates the visible cross section for experimental data with an optimal curve for the Fit 1.

From Table 2 good fit quality can be seen for both approximations. The Fit 1 was chosen as the main one, with both statistical (first) and systematic (second) uncertainties shown for its optimal parameters.

To determine the 3π Born cross section, the radiative correction was calculated according to Eq. (3) and then applied to the experimental values of the visible cross section

$$\sigma_{\rm B}(s) = \sigma_{\rm vis}(s)/\big(1+\delta_{\rm rad}(s)\big). \quad (5)$$

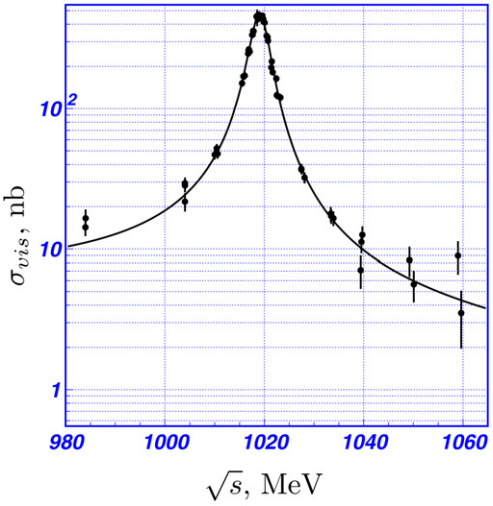

Fig. 4. Visible cross section with an optimal curve for the Fit 1 (see Table 1).

To calculate an additional uncertainty related to the radiative corrections, we performed toy MC simulation of the Born cross section shape determined by the fit parameters.

7. Analysis of $\phi \to \pi^+\pi^-\pi^0$ dynamics

For this analysis the Dalitz plot in $X = \frac{E_{\pi^-} - E_{\pi^+}}{\sqrt{3}}$ and $Y = \sqrt{s} - E_{\pi^-} - E_{\pi^+} - m_{\pi^0}$ variables was used. The kinematicaly allowed region was divided into 198 square bins of 20×20 MeV size. 79 577 experimental 3π events from the c.m. energy range $\sqrt{s} = 1017$–1021 MeV were selected for this analysis. In this c.m. energy region background is about 1%, and its influence was found to be negligible. In addition to the selection criteria mentioned in Section 3, a constrained fit taking into account total energy–momentum conservation was applied.

To fit the Dalitz plot distribution, a model incorporating the $\rho\pi$ mechanism and non-$\rho\pi$ contribution described by a contact amplitude was used. The expected number of events in the bin number k is given by expression

$$N_k^{\rm th} = N_0 \int_k dX\, dY\, |\vec{P}_+ \times \vec{P}_-|^2 \big|A_n a e^{i\varphi} + A_{\rho\pi}\big|^2, \quad (6)$$

where: N_0—normalization parameter proportional to the total number of 3π events, $A_{\rho\pi}$—$\rho\pi$ contribution to the amplitude determined from formula

$$A_{\rho\pi} = \frac{1}{D_{\rho^+}(Q_+^2)} + \frac{1}{D_{\rho^-}(Q_-^2)} + \frac{1}{D_{\rho^0}(Q_0^2)}, \quad (7)$$

where the ρ^i-meson ($i = +, -, 0$) propagator is written in the form

$$\frac{1}{D_{\rho^i}(Q_i^2)} = \frac{1}{\frac{Q_i^2}{M_\rho^2} - 1 + i\frac{\sqrt{Q_i^2}\Gamma_\rho(Q_i^2)}{M_\rho^2}}. \quad (8)$$

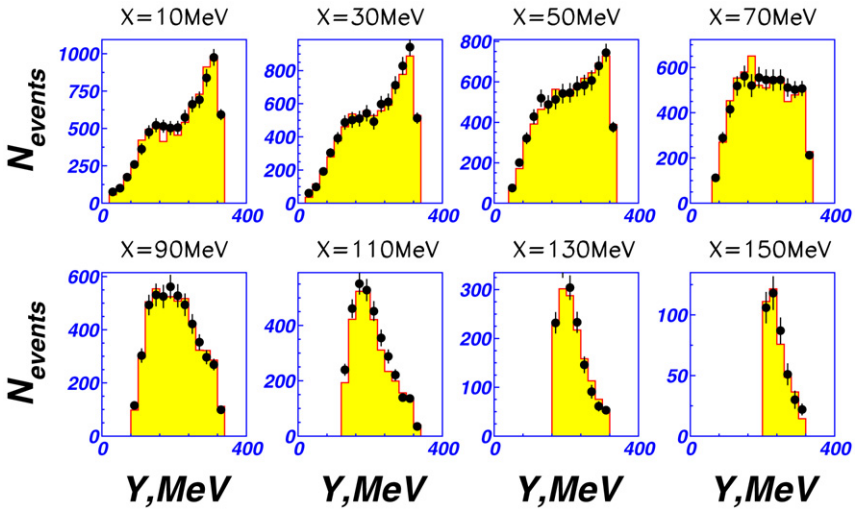

Fig. 5. Result of the fit. Slices of the Dalitz plot distribution (right half) along the Y axis for different values of X are shown. Points are experimental data, histogram—calculated numbers.

The non-$\rho\pi$ amplitude includes: a normalization coefficient $A_n = 7.52$ determined by expression

$$\int\limits_{\text{Dalitz}} dX\,dY\,|\vec{P}_+ \times \vec{P}_-|^2 |A_{\rho\pi}|^2 = |A_n|^2 \int\limits_{\text{Dalitz}} dX\,dY\,|\vec{P}_+ \times \vec{P}_-|^2, \tag{9}$$

an absolute value of the normalized contact amplitude a and a phase of the contact amplitude φ. The calculated number of events in the ith cell is given by expression:

$$N_i^{\text{calc}} = \varepsilon_{ik} N_k^{\text{th}}, \tag{10}$$

where ε_{ik} is 198×198 matrix of the detector apparatus function. Due to the non-ideal reconstruction and finite resolution of the detector, a 3π event initially produced in the bin number k can be found in the bin number i, so along with the detection efficiency for every bin, ε_{ik} provides a matrix of bin-to-bin transition probabilities. It also takes into account the effect of Dalitz plot distortion due to the initial state radiation. Full 3π MC simulation with initial state radiation was used to extract ε_{ik}.

To approximate the Dalitz plot distribution we minimize the χ^2 function

$$\chi^2 = \sum_{i=1}^{198} \frac{(N_i^{\text{exp}} - N_i^{\text{calc}})^2}{N_i^{\text{exp}} + \sigma_i^2(N^{\text{calc}})}, \tag{11}$$

where: N_i^{exp}—number of experimental events, N_i^{calc}, $\sigma_i(N^{\text{calc}})$—calculated number of events and its error. Free parameters of the fit are: N_0, a and φ. Fig. 5 shows cuts along the Y axis for different X values of the experimental Dalitz plot distribution (points) and fit result (histograms). The obtained optimal parameters are given in Table 3. Also shown are the values of the contact term found by KLOE[1] [12], SND [7], and CMD-2 [6] groups. The higher resonances like $\rho(1450)$ or $\rho(1700)$ can contribute to the non-$\rho\pi$ term as well. Under the assumption that the non-$\rho\pi$ amplitude is dominated by the $\rho(1450)\pi$ mechanism the expected number of events in the bin number k of the Dalitz plot is given by expression (similar to Eq. (6))

$$N_k^{\text{th}} = N_0 \int\limits_k dX\,dY\,|\vec{P}_+ \times \vec{P}_-|^2 \left|A_{\rho'\pi} a' e^{i\varphi'} + A_{\rho\pi}\right|^2, \tag{12}$$

where the term $A_{\rho'\pi} a' e^{i\varphi'}$ appears instead of the contact amplitude and describes the $\rho'\pi$ contribution

$$A_{\rho'\pi} = \frac{1}{D_{\rho'^+}(Q_+^2)} + \frac{1}{D_{\rho'^-}(Q_-^2)} + \frac{1}{D_{\rho'^0}(Q_0^2)}, \tag{13}$$

where $\frac{1}{D_{\rho'^i}(Q_i^2)}$ is the ρ'^i-meson ($i = +, -, 0$) propagator determined by the equation similar to Eq. (8). Parameters of the $\rho(1450)$ were taken from [19]: $M_{\rho'} = 1465 \pm 25$ MeV/c^2 and $\Gamma_{\rho'} = 400 \pm 60$ MeV. The admixture of the $A_{\rho'\pi}$ is described by the complex constant $a' e^{i\varphi'}$, its absolute value is related to the hadronic coupling constants as

$$a' = \frac{g_{\phi\rho'\pi}\, g_{\rho'\pi\pi}}{g_{\phi\rho\pi}\, g_{\rho\pi\pi}}. \tag{14}$$

Table 3
Results on the absolute value and phase of the contact amplitude

CMD-2 This work	$a = 0.101 \pm 0.044_{\text{stat}} \pm 0.017_{\text{sys}}$ $\varphi = -2.91 \pm 0.14_{\text{stat}} \pm 0.07_{\text{sys}}$ $\chi^2/\text{Ndf} = 0.95$ significance 3.3σ
KLOE (2003)	$a = 0.104 \pm 0.010_{\text{stat}} \pm 0.020_{\text{sys}}$ $\varphi = -2.47 \pm 0.08_{\text{stat}} \pm 0.08_{\text{sys}}$
SND (2002)	$-0.06 < a < 0.06$ $\varphi = 0$-fixed; 90% CL
CMD-2 (1998)	$-0.15 < a < 0.10$ $\varphi = 0$-fixed; 90% CL

[1] In [12, p. 8] $A_{\text{dir}} = a_d e^{i\phi_d}$ should be read as $A_{\text{dir}} = a_d e^{-i\phi_d}$—private communication with Dr. C. Bini.

Free parameters of the fit were: N_0, a' and φ'. The obtained values are: $a' = 0.215 \pm 0.092 \pm 0.036$ and $\varphi' = 0.177 \pm 0.132 \pm 0.051$, where the first error is statistical and the second is systematic.

8. Systematic uncertainties

The systematic uncertainty on the ϕ-meson mass—m_ϕ is evaluated to be 0.1 MeV dominated by the energy determination procedure. The systematic uncertainties on the total ϕ-meson width—Γ_ϕ and ϕ–ω interference phase—$\varphi_{\phi-\omega}$ were evaluated approximating cross section data for three different energy scans, and found to be 0.17 MeV and 10°, respectively. The dominant contribution to the $\sigma_{3\pi}$ systematic uncertainty comes from the uncertainty on the integrated luminosity (2%). The systematic uncertainty on the radiative corrections is determined by the efficiency function $\varepsilon(x_1, x_2)$ error ($\approx 1\%$) and theoretical uncertainty of the method itself (0.2%) [18]. The systematic uncertainty on the detection efficiency consists of a 0.4% uncertainty due to the limited 3π MC statistics, 0.3% uncertainty on the track efficiency correction and 0.2% uncertainty on the π^0 efficiency correction. We assigned a 1% systematic uncertainty related to the trigger efficiency. The 0.3% systematic uncertainty due to the background subtraction was found applying two different background subtraction procedures. A total uncertainty of 2.5% was obtained by adding all the contributions in quadrature.

The systematic uncertainties on the value of the contact amplitude come from the non-uniformity of the detection efficiency over the Dalitz plot—0.017 for a and 0.07 for φ; the uncertainty on the ρ-meson parameters—0.003 for a and 0.03 for φ. The model uncertainty was evaluated applying two different parametrizations of the ρ-meson shape—relativistic Breit–Wigner and Gounaris–Sakurai formula [22]. This difference was found to be negligible. The total systematic uncertainty was obtained by adding all the contributions in quadrature.

9. Conclusions

The cross section of the process $e^+e^- \to \pi^+\pi^-\pi^0$ was measured in the c.m. energy range from 984 to 1060 MeV. The mass and width of the ϕ-meson as well as ω–ϕ mixing phase are shown in the second column of Table 2. They do not contradict to the world average values [19]. Our result on the 3π peak cross section is

$$\sigma_{3\pi} = (637 \pm 23_{\text{stat}} \pm 16_{\text{syst}})\ \text{nb}.$$

We calculate the product of the $\phi \to \pi^+\pi^-\pi^0$ branching ratio and $\phi \to e^+e^-$ $B_{ee}B_{3\pi}$ according to the relation

$$B_{ee}B_{3\pi} = \frac{\sigma_{3\pi} M_\phi^2}{12\pi} = (4.51 \pm 0.16 \pm 0.11) \times 10^{-5}. \quad (15)$$

Our result is in good agreement with the previous measurements coming from CMD-2 [6], SND [20] and BaBar [21] and has the best total accuracy.

Dalitz plot analysis showed good agreement between the CMD-2 and KLOE results, see Table 3. The determined value of the non-$\rho\pi$ amplitude is consistent with the theoretical estimations of the contact term [8,9]. Under the assumption that the non-$\rho\pi$ amplitude is dominated by the $\rho(1450)\pi$ mechanism the ratio of the hadronic coupling constants was extracted: $\frac{g_{\phi\rho'\pi} g_{\rho'\pi\pi}}{g_{\phi\rho\pi} g_{\rho\pi\pi}} = 0.215 \pm 0.092 \pm 0.036$.

Acknowledgements

The authors are grateful to the staff of VEPP-2M for excellent performance of the collider, to all engineers and technicians who participated in the design, commissioning and operation of CMD-2. This work was supported in part by grants PST.CLG.980342, RFBR-03-02-16280, RFBR-03-02-16477, RFBR-03-02-16843, RFBR-04-02-16217, RFBR-04-02-16223, RFBR-04-02-16434, and Sci. School-905.2006.2.

References

[1] G.A. Aksenov, et al., Preprint Budker INP 85-118, Novosibirsk, 1985.
[2] E.V. Anashkin, et al., ICFA Inst. Bull. 5 (1988) 18.
[3] V.V. Anashin, et al., Preprint Budker INP 84-114, Novosibirsk, 1984.
[4] M. Gell-Mann, D. Sharp, W.G. Wagner, Phys. Rev. Lett. 8 (1962) 261.
[5] G. Parrour, et al., Phys. Lett. B 63 (1976) 362.
[6] R.R. Akhmetshin, et al., Phys. Lett. B 434 (1998) 426.
[7] M.N. Achasov, et al., Phys. Rev. D 65 (2002) 032002.
[8] Y. Brihaye, N.K. Pak, P. Rossi, Nucl. Phys. B 254 (1985) 71.
[9] O. Kaymakcalan, S. Rajeev, J. Schechter, Phys. Rev. D 30 (1984) 594.
[10] E.A. Kuraev, Z.K. Silagadze, Phys. At. Nucl. 58 (1995) 1589.
[11] T. Fujiwara, et al., Prog. Theor. Phys. 73 (1985) 926.
[12] A. Aloisio, et al., Phys. Lett. B 561 (2003) 55.
[13] D. Epifanov, in: Proceedings of the International Conference DAΦNE 2004: Physics at Meson Factories, Frascati, June 2004, p. 389.
[14] S. Eidelman, F. Jegerlehner, Z. Phys. C 67 (1995) 585.
[15] N.N. Achasov, et al., Int. J. Mod. Phys. A 7 (1992) 3187.
[16] R.R. Akhmetshin, et al., Phys. Lett. B 466 (1999) 392.
[17] R.R. Akhmetshin, et al., Preprint Budker INP 2006-28, Novosibirsk, 2006.
[18] E.A. Kuraev, V.S. Fadin, Sov. J. Nucl. Phys. 41 (1985) 466.
[19] S. Eidelman, et al., Phys. Lett. B 592 (2004) 1.
[20] M.N. Achasov, et al., Phys. Rev. D 63 (2001) 072002.
[21] B. Aubert, et al., Phys. Rev. D 70 (2004) 072004.
[22] G.J. Gounaris, J.J. Sakurai, Phys. Rev. Lett. 21 (1968) 244.